International Symposium
On Turbulence and Shear Flow
Phenomena (TSFP-8)
August 28 - 30, 2013 Poitiers, France

FEEDBACK CONTROL FOR LAMINARIZATION OF FLOW OVER WINGS

Reza Dadfar
Linné Flow Centre, KTH Mechanics SE-100 44 Stockholm, Sweden
dadfar@mech.kth.se

Ardeshir Hanifi[1,2] **and Dan S. Henningson**[1]
[1]Linné Flow Centre, KTH Mechanics SE-100 44 Stockholm, Sweden
[2] Swedish Defense Research Agency, FOI, SE-164 90 Stockholm, Sweden

ABSTRACT

An output feedback controller is designed to attenuate the amplitude of the Tollmien-Schlichting (TS) waves inside the boundary layer of an airfoil. The dynamics of the system are modelled by the linearised Naiver-Stokes equation. The impulse response to a generic initial condition is investigated. The perturbation evolves and penetrates inside the boundary layer and triggers the TS waves. A linear Gaussian controller based on the reduced order model is designed where the sensors and actuates are localised near the wall. An output projection is used to identify the unstable disturbances and the modes with large energy content in the TS wave frequency band; the objective function of the controller is selected as a set of Proper Orthogonal Decomposition (POD) modes. A plasma actuator is modelled and implemented as an external forcing on the flow. To account for the limitation of the plasma actuators several strategies are examined. The results are compared with an ideal LQG controller where the constraints are not accounted for the control design. The outcomes reveal successful performance in mitigating the amplitude of the wavepacket developing inside the boundary layer.

Introduction

The hydrodynamic drag on an immersed body increases while the flow experiences a transition from laminar to turbulence. Delaying this transition can positively influence the operational costs of vehicles and aircraft; in fact, it can reduce the fuel consumption and consequently mitigate the environmental pollutions. The transition on an unswept wing of an aircraft is initiated by the Tollmien-Schlichting (TS) waves (Kachanov, 1994) which grow exponentially as they evolve inside the boundary layer. Delaying the transition can be achieved by attenuating the amplitude of these waves. Here, we used an active control strategy to accomplish that aim.

The early work on the combination of fluid dynamics and control theory dates back to the paper by Joshi *et al.* (1997). We refer to Kim & Bewley (2007) for a recent review on this topic. In the flow problems, the discretisation of the Navier-Stoke equation results in a high dimensional system with large degrees of freedom. Hence, it is difficult to apply the classical control design methodology in an efficient manner. This difficulty can be addressed by identifying a low dimensional model that preserves the essential dynamics of the original dynamical system. Once this model is available a low order controller can be designed using the classical control techniques. This approach is usually referred to as *reduce-then-design* (see Anderson & Liu (1989)).

A systematic way to obtain the reduced-order model (ROM) is the Galerkin projection of the Navier-Stokes system onto a set of modes. The choice of these modes is essential to the property of the resulting reduced-order model. The balance truncation is introduced by Moore (1981) and an approximation based on the snapshot method is proposed by Rowley (2005) which is referred to as balanced POD method (BPOD). A limitation of the method is that the adjoint solution should be available. System identification techniques allow us to circumvent this restriction; a reduced-order model of the system can be computed by only the measurement extracted directly from the flow. An example is represented by the Eigensystem Realisation Algorithm (ERA) first introduced by Juang & Pappa (1985) The results of this algorithm are theoretically equivalent to BPOD.

A crucial aspect of an active control system is the choice of the actuator. Among different types of the actuator, plasma actuators have gained a lot of interest due to their simplicity, low power consumption, higher frequency response and lack of any moving parts. These characteristics make them convenient for being used in experimental environments; for a review, we referred to Corke *et al.* (2009). One of the well-known variant of plasma actuator is the single dielectric barrier discharge which has been implemented successfully to delay the transition in an experimental setup (see Grundmann & Tropea (2008)).

In this paper, we implemented a model that reproduces the force distribution of the plasma actuator, already used in previous experimental investigations (Kriegseis, 2011). The resultant force is oriented along only one direction. This cast a constraint on the LQG controller design. In this work, we investigate several strategies to attack these limitations.

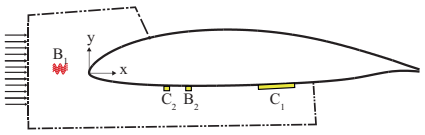

Figure 1. Configuration of the sensors and actuators. The initial perturbation B_1 is located at $(x,y) = (-1.5,-0.5)$. The actuator B_2, located at $0.33c$, equivalent to $(36.67,-4.38)$ where the chord length is indicated by c; the estimation sensor C_2 is placed at $0.31c$, equivalent to $(34.45,-4.42)$; the controller is designed based on the measurement extracted by the output C_1, constituted by 12 proper orthogonal decomposition(POD) modes, computed over a region that extends approximately from $x = 36$ to $x = 70$.

1 Flow Configuration and Governing Equations

A two dimensional (2D) viscous incompressible flow developing over an airfoil at angle of attack $\alpha = -0.7^o$ is considered. The geometry is used previously by Reed *et al.* (2013) in the flight experiments. The configuration is depicted in Fig. 1. The dynamics of small amplitude perturbations is governed by Navier-Stokes equation linearised around a base flow.

$$\frac{\partial u}{\partial t} = -(U\cdot\nabla)u - (u\cdot\nabla)U - \nabla p + \frac{1}{Re}\nabla^2 u \qquad (1a)$$

$$\nabla\cdot u = 0, \qquad (1b)$$

$$u = u_0 \quad \text{at} \quad t = t_0, \qquad (1c)$$

where the disturbance velocity and pressure fields are denoted by $u(x,y,t)$ and $p(x,y,t)$, respectively, while x denotes the horizontal direction and y the vertical one (*see* Fig. 1). $U(x,y)$ and $P(x,y)$ represent the baseflow velocity and pressure, respectively. In this study, all the spatial coordinates are normalised with the noise radius, r of the airfoil. The discretised linearised Navier-Stokes equations with boundary conditions can be written in state space form as the following initial value problem (Bagheri *et al.*, 2009)

$$\frac{du}{dt} = Au, \quad u(t_0) = u_0, \qquad (2)$$

where A is the discretised linearised Navier-Stokes operator and u is the discretised velocity field.

1.1 Numerical Simulations

Direct Numerical Simulations (DNS) of the flow on an airfoil are performed using spectral element method (SEM). This technique provides both the geometrical flexibility of the finite element and the accuracy of spectral method. The simulation code is Nek5000 developed by Paul F. Fischer & Kerkemeier (2008). The spatial domain is decomposed into finite elements which in turn are divided into arrays of Gauss-Lobatto-Legendre (GLL) nodes. The solution of Navier Stokes equation in each element is defined as a linear combination of Lagrange interpolant defined by an orthogonal Legendre polynomial as a basis of degree N. A staggered grid of lower order, $N-2$, for the pressure is adopted. The method is called $P_N - P_{N-2}$ (Maday & Patera, 1989). The polynomial order of $N = 5$ is adopted in this investigation. For the time integration a second order Adam-Bashforth scheme is employed.

1.2 Baseflow and perturbation

The baseflow is computed by matching the full Navier-Stokes system in time until the solution is steady. The reference speed is the free stream velocity $U_\infty = 39m/s$ and the reference length is the nose radius of the airfoil r. The flow conditions are defined by the Reynolds number defined as $Re_r = U_\infty r/\nu = 25094$ with $\nu = 1.86\times10^{-5}m^2/s$ being the kinematic viscosity. The Reynolds number based on the chord length is $Re_c = U_\infty c/\nu = 2.8\times10^6$ where $c = 1.35m$, is the chord length of the airfoil. No-slip conditions are prescribed along the airfoil, while Neumann boundary conditions are applied at the outflow. The far-field boundary (inflow plane and free-stream) is of Dirichlet type, computed by solving the Reynolds-Average Navier-Stokes equation over the airfoil in a square box extended from $x,y \in [-100\ 100]\ m$. To correct the pressure distribution along the airfoil a numerical sponge is applied at the outflow of the domain where the DNS velocities are forced to the RANS solution. The domain is discretised into 24326 spectral finite elements, formed by 36 GLL points each. The elements are clustered near the wall where the boundary layer effects are crucial and the sensor and actuator are located. The perturbation evolution is governed by the Linearised Navier-Stokes (LNSE) equations, (see Eq. 1). The computational domain is the same already introduced for the baseflow computations. The boundary conditions along the walls and for the outflows are of the same type already introduced, meanwhile null Dirichlet boundary conditions is imposed in the far-field (inflow and free-stream). These boundary conditions are applied far enough from the boundary layer to have negligible effects on the perturbation evolution.

2 Input-Output System

A schematic representation of the input-output configuration is depicted in Fig. 1 where a sketch of the airfoil together with the inputs and outputs are presented. In this setup, d disturbances, m localised actuators and p estimation sensors are considered. The discretised Navier-Stokes equation with the inputs and outputs can be formulated in state space form as

$$\dot{u} = Au + Bf, \qquad (3a)$$

$$y = Cu + Df, \qquad (3b)$$

where

$$B = (B_1, 0, B_2), C = \begin{pmatrix} C_1 \\ C_2 \end{pmatrix}, D = \begin{pmatrix} 0 & 0 & I_l \\ 0 & I_\alpha & 0 \end{pmatrix}, f(t) = \begin{pmatrix} w(t) \\ g(t) \\ \phi(t) \end{pmatrix},$$

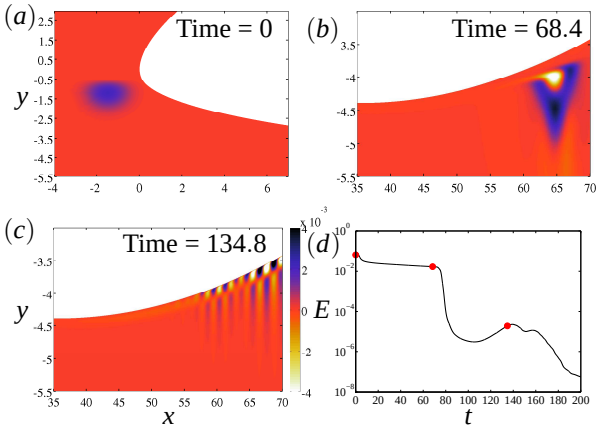

Figure 2. Impulse response of the system to an initial perturbation B_1; the streamwise velocity of the disturbance is shown at different instants of time, $t = [0, 68.4, 134.8]$. Furthermore, the energy of the system is shown as a function of time. For visualisation purpose, we multiply the amplitude of the perturbations in (a) and (b) by 100 and 25 respectively.

and

$$y(t) = \begin{pmatrix} z(t) \\ v(t) \end{pmatrix}.$$

The matrix $A \in \mathbb{R}^{n\times n}$ represents the linearised and discretised Navier-Stokes equation and $D \in \mathbb{R}^{(k+p)\times(d+m+1)}$. The inputs are introduced through the forcing term Bf, where the inputs $B \in \mathbb{R}^{n\times(d+m+1)}$ and $f(t) \in \mathbb{R}^{(d+m+1)}$. In particular, $B_1 \in \mathbb{R}^{n\times d}$ is an external disturbance located in front of the airfoil with the corresponding temporal part, $w(t)$; we only assume one disturbance $d = 1$ in this setup. The other inputs $B_2 \in \mathbb{R}^{n\times m}$ represent m actuators located inside the boundary layer, fed by the control signals $\phi(t) \in \mathbb{R}^m$. The output signals are contained in vector $y(t) \in \mathbb{R}^{k+p}$ and are detected by $C \in \mathbb{R}^{(k+p)\times n}$. We can write the outputs as

$$z(t) = C_1 u(t) + I_l \phi(t), \tag{4a}$$
$$v(t) = C_2 u(t) + I_\alpha g(t), \tag{4b}$$

where the measurements $v(t)$ provide information about the travelling structures detected by sensors C_2. These measurements are corrupted by the white noise signals $I_\alpha g(t)$ with a covariance α; in detail, $g(t) \in \mathbb{R}$ is a white noise signal with the unit covariance and I_α is a matrix with α on the diagonal entries. The second output signals $z(t) \in \mathbb{R}^k$ extracts information via k outputs $C_1 \in \mathbb{R}^{k\times n}$ placed far downstream in the computational box; it is used to design and assess the performance of the controller. The matrix $I_l \in \mathbb{R}^{k\times m}$ contains the control penalty l in each diagonal entry and can be regarded as the control cost.

2.1 Initial perturbation

The upstream perturbation B_1 is a localised disturbance placed in front of the airfoil and outside of the boundary layer. It is chosen as a Gaussian disturbance defined as

$$h(x,y) = \begin{pmatrix} \sigma_x \gamma_y \\ -\sigma_y \gamma_x \end{pmatrix} exp(-\gamma_x^2 - \gamma_y^2), \tag{5}$$

where

$$\gamma_x = \frac{x - x_0}{\sigma_x}, \quad \gamma_y = \frac{y - y_0}{\sigma_y}. \tag{6}$$

and (x_0, y_0) is the centre of the Gaussian distribution. The scalar quantities are $\sigma_x = 1$, $\sigma_y = 1$, $x_0 = -1.5$ and $y_0 = -0.5$.

The evolution of the disturbance is depicted in Fig. 2, where the impulse response of the system to the initial condition for three different instants together with the energy of the system is shown. The perturbation is mostly localised into two different regions, inside and outside of the boundary layer. The outer perturbation is a large energetic structure moves faster, with a velocity close to the free stream velocity (U_∞); the amplitude of this perturbation decreases meanwhile it is advected downstream. When this structure leaves the observation windows at time $t \approx 100$, inside the boundary layer, the Tollmien-Schlichting (TS) wavepacket is observed, which develops together with longer structures stretched along the streamwise direction (see Fig. 2). The TS wavepacket moves slower but it is convectively unstable; indeed, it grows meanwhile evolving along the streamwise direction and hence the energy of the system increases. Thus, this perturbation is the most interesting for the analysis of the transition process.

2.2 Actuator

In this setup, we use a model of the plasma actuator. Fig. 3 indicates a schematic diagram of this actuator. It consists of two electrodes, one exposed and one encapsulated in the surface connected to an AC voltage source and separated by a dielectric material. If the voltage increases enough, the air above the dielectric material is ionised and consequently, ions accelerate in the presence of the electrical fields and collide with the neutral particle of the air. The overall effect of this process is to produce a body force ((Mertz & Corke, 2011, see)). One approach to model the effects of the plasma actuator on the flow is to compute the produced body force (Kriegseis, 2011); the spatial distribution of the force is not constant and usually depends on the supplied voltage and frequency. This violates the assumption of time invariance of the system in LQG framework. In this study, we use the force distribution obtained with a supply source at 10kV voltage. Dadfar *et al.* (2013) investigated the effect of scaling the spatial distribution of the force at 10kV and found a negligible influence on the overall performance of a LQG controller. Moreover, with predetermined electrodes location, the plasma actuator produces force in only one direction. This dictates a constraint on the design of LQG controller which will be discussed accordingly.

2.3 Sensors and objective function

The measurement from the flow are extracted by the sensor C_2 ($p = 1$) and outputs C_1 ($k = 12$). The measurement signal from sensor C_2, $v(t)$ in Eq. 4b is used for the estimation and placed a short distance upstream of the actuator B_2. The measurements in C_2 are extracted by averaging the velocity filed using the Gaussian function (Eq. 6) as

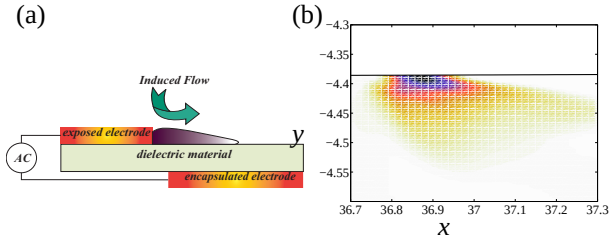

Figure 3. (a) a schematic view of Single Dielectric Barrier Discharge (SDBD) plasma actuator (b) force distribution for the plasma actuator.

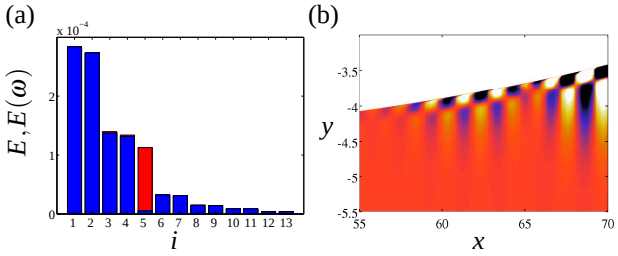

Figure 4. (a) The energy of each pod mode E_i and the corresponding energy $E(\omega)$ in the frequency range $0.5 < \omega < 2$. (b) The streamwise velocity component of the first POD mode $i = 1$.

weight. Moreover, since it always accompany with noise, a white noise with a level of α is assumed to corrupt the measurement. A high value of α introduces high level of contamination while a low value indicates high fidelity of the data. The output signal $z(t)$ is used to assess the performance of the controller. The minimisation of the output signal detected in C_1 is the objective of our LQG controller. Indeed, the aim is to find a control signal $\phi(t)$ able to attenuate the amplitude of the disturbance detected by C_1. Hence, the objective function reads

$$\|z\|^2_{L^2_{[0,\infty]}} = \int_0^\infty \|C_1 u\|_2^2 + l^2 \|\phi\|_2^2 \, \mathrm{d}t, \qquad (7)$$

where l is the control penalty and represents the expense of the control. This parameter is introduced as a regularization term accounting for physical restrictions. Large values of control penalty result in weak actuation and creates low amplitude control signal whereas low values of control penalty lead to strong actuation. The output C_1 is represented by a basis of proper orthogonal decomposition (POD) modes. Selecting the most energetic POD modes as the basis of the objective function C_1, allows us to identify the most energetic structures and obtain a low-order approximation of the original system. This is the so-called output projection (Rowley, 2005). In this setup, 13 POD modes are considered where they totally capture 99% of the flow energy. The energy content of each mode is represented in Fig. 4a. Since we are only interested to suppress the amplitude of the TS waves, we only aim to identify and attenuate the amplitude of the energetic structures with enormous energy content in frequency band $0.5 < \omega < 2$. Hence, we exclude the mode number 5 and use the other 12 POD modes as the objective function.

Model order reduction and control design

The control design follows the same steps introduced in Dadfar *et al.* (2013), where the control of 2D perturbations are investigated within the linear framework. The *reduce-then-design* scheme (Anderson & Liu, 1989) is implemented. First, a reduced-order model is obtained using the Eigensystem Realisation Algorithm (ERA), using that model a Linear Quadratic Gaussian (LQG) controller is designed based on the reduced-order model. To account for the limitation of the plasma actuator concerning its inability to provide force in both directions, two different strategies are under investigation in this paper (for more detailed and mathematical derivation see Dadfar *et al.* (2013)). First, the control design is performed by considering a model with a baseflow modified by a constant forcing; indeed, the baseflow is added to the one resulting from a constant forcing; from the theoretical point of view, the linearisation is performed on a modified equilibrium state. Next, the control design is performed on the modified baseflow; once the control design is completed, the forcing appears in the control term as an offset of the control law. By introducing this procedure, the control law provides an action around a mean value and results to be only positive (or negative). Because of this limitation, hereafter this strategy is referred to as *constrained controller with an offset*. In a different attempt, two actuators are employed, designed for acting in opposite directions; First, a LQG optimal controller is designed for the first actuator; we apply a proper saturation function such that the positive control signal is truncated and only the negative signal is fed into the actuator. This is analogous to apply forcing only in negative direction. Once the first closed loop is adjusted, we design a second LQG controller for the second actuator; we based the design on the first closed loop, such that we can attenuate the amplitude of the wavepacket once that first controller has been already activated. Also in this case, a saturation function is applied and only the positive part of the signal is fed into the controller.

3 Results

In this section several control strategies are compared and discussed.

3.1 LQG controller

In this section, the performance of the closed-loop system is evaluated using plasma actuator. The design parameters including control penalty and noise variance are chosen as case A in table 1. Moreover, this case is considered as the reference case in this investigation. Fig. 5 represents an example of the spatial distribution of the streamwise perturbation velocity for uncontrolled (5a) and controlled case (5b) at time $t = 128$. It can be observed that the high frequency structures are faded considerably specially at the end of the domain. The maximum streamwise velocity is also attenuated up to 91%. Fig. 6 presents the closed-loop behaviour of the system from the input-output point of view (case A). In the first inset 6a, the measurement detected by the upstream sensor C_2 is reported. The sensor placed close to the wall so it can only register the disturbances evolving inside the boundary layer. At the time interval $t \in [40,\ 60]$, the signals are related to the structures moving fast with the free stream velocity U_∞ at the edge of the boundary layer penetrating inside the boundary layer.

Table 1. The performance for different cases is depicted. Each case corresponds to a different choice of controller; LQG controller (A); Constrained controller with an offset (B); Two adjacent controllers (C); Constrained controller without an offset (D). The control penalty and noise covariance for all the cases are assumed as $l = 10^{-1}$ and $\alpha = 10^{-2}$ respectively. The norms are computed for the time $t > 80$.

Case	System norm	Norms Ratio
-	$\| G \|_2^2$	$\frac{\|G_{con}\|_2^2}{\|G_{unc}\|_2^2}$
NC	1.2×10^{-1}	–
A	5.3×10^{-3}	4.2%
B	5.3×10^{-3}	4.2%
C	1.5×10^{-2}	11.8%
D	4.3×10^{-2}	34.4%

They eventually trigger the TS wavepacket moving slower observed at time interval $t \in [70, 90]$. After the wavepacket is convected past the sensor, the signal is faded out and tends to zero . In Fig. 6b, the control signal feeding the actuator B_2 is depicted. The first part of the signal $t<70$ is related to the fast moving structure while the second part $t>70$ is associated with the wavepacket and indicates the controller attempts to damp the amplitude of the wavepacket. As it can be seen, even though the controller is not perfectly insensitive to the free-stream perturbation, it puts more effort to attenuate the amplitude of the wavepacket while it is several order of magnitude smaller than the free-stream perturbations. Fig. 6c and 6d report the time signals detected by output sensors $C_{1,1}$ and $C_{1,3}$. They are also resembling the time coefficient of the first and third POD modes. The red line indicates the uncontrolled case while the blue lines represent the controlled case. The controller can successfully attenuate the amplitude of these modes. To further investigate the performance of the controller, a second quantitative analysis, is to investigate the energy of the wavepacket in time domain for the uncontrolled and controlled cases. Fig. 7 depicts the energy of the wavepacket for the uncontrolled case (red line). It can be observed that the energy increases as the wavepacket evolves. The reason relies on the fact that the flow is convectively unstable and the wavepacket includes a collection of the TS waves. The energy of the system for the controlled case is also reported in blue lines. The controller can attenuate the maximum energy of the wavepacket up to 93.1% which indicates a corresponding suppression of the wavepacket amplitude.

3.2 Constrained controller

The constrained controller is introduced to overcome the limitation of the plasma actuator which can only deliver force in one direction. Two constrained controllers with and without an offset are presented in this investigation. The former (case B) is designed as the following: a constant control signal $\bar{\phi} = 5 \times 10^{-3}$ is applied and on the top of that an optimal control signal is introduced, such that the sum of the two signals is positive. The latter is a LQG controller where simply a saturation function is applied on its control signal and the positive part of the signal is truncated (case D). Fig. 7 presents the energy of the perturbations for different control strategies. The red dots and solid black line indicate the first and the second controllers respectively while the solid blue line resembles the reference case. The performance of the case without an offset (case *D*) is poor compared to the other two controllers. In fact, it can attenuate the maximum energy of the wavepacket up to 61.7% meanwhile the first controllers, case B, can mitigate the energy up to 93.1%. Furthermore, the first and LQG controller performed similarly. The similarity stems from the fact that a perturbation with zero frequency is added to the baseflow and the resultant modification is quite small. Hence the energy of the perturbations on the original and modified baseflow acts practically in the same way.

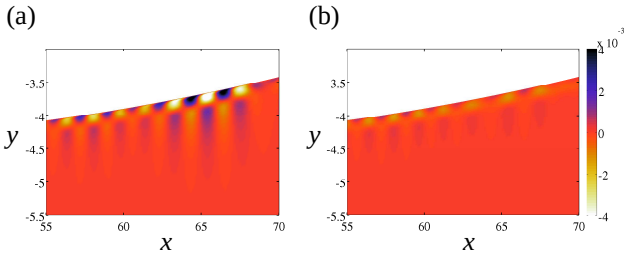

Figure 5. Streamwise perturbation velocity profiles; (a) uncontrolled and (b) controlled case at time $t = 128$.

3.3 Two adjacent controllers

Two adjacent controllers are implemented and located at the $x = 36.68$ and $x = 37.20$ respectively. This control strategy does not result in an optimal controller and the performance deteriorated as the distance between the two actuators increases compared to a case when they are on the top of each other even though, the latter configuration is almost impossible due to the practical implementation. Fig. 7 reports the energy of the system using this strategy. The results reveal that two adjacent controllers could attenuate the maximum energy of the wavepacket up to 84.4% compared to 93.1% reduction in an optimal LQG controller.

3.4 Conclusion

An output feedback controller is designed on a 2D airfoil in order to suppress the amplitude of TS waves in combination with the plasma actuator. The linearised Navier Stokes equation is considered to represent the dynamics of the system. The impulse response to an initial perturbation is investigated and modelled as a generic disturbance represented by a Gaussian function located in front of the airfoil and outside of the boundary layer. The perturbation is advected downstream and penetrates inside the boundary layer and triggers the TS waves. A Linear Quadratic Gaussian (LQG) controller based on a reduced-order model is designed using a system identification approach via Eigensystem Realisation Algorithm (ERA). The controller relies on the information provided via a localised estimation sensor upstream of the actuator. A set of POD modes characterising the dynamics of the wavepacket is introduced as an objective function of the controller and a model of a single dielectric plasma actuator is implemented. Due to the specific configuration of the plasma actuator they can only provide force in one direction. We investigated these limitations by studying several strategies. First, we constrained the controller to act only in one direction by simply truncat-

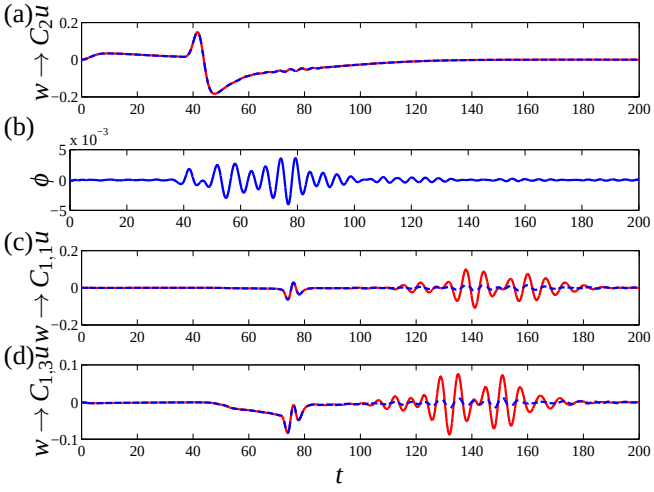

Figure 6. Impulse response of the system. (a) Signal from input B_1 to sensor C_2. (b) Control signal feeding the actuator B_2. (c) Measurements extracted by sensor $C_{1,1}$ and (d) sensor $C_{1,3}$. The solid red lines indicate the reference case without control while the blue lines represent the controlled case.

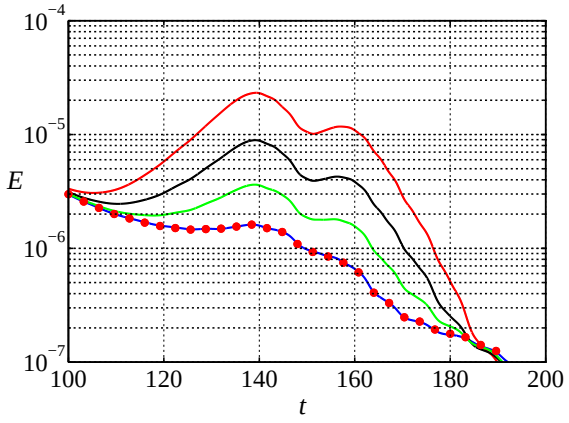

Figure 7. Energy of the perturbations in different cases; red, black, green and blue lines indicate the uncontrolled case, constrained controller without an offset, two adjacent controllers and LQG controller respectively; the dotted red line represents the constrained controller with an offset.

ing the control signal; next, we introduced an offset to the control signal by adding a constant actuation; this method results in an optimal controller and performs as well as a classical LQG controller. Finally; we used two adjacent controllers acting in opposite directions only; although this method is more expensive in terms of hardware, the performance was quite acceptable. The performance of the case with an offset was the best in comparison to the other controllers.

REFERENCES

Anderson, Brian DO & Liu, Yi 1989 Controller reduction: concepts and approaches. *Automatic Control, IEEE Transactions on* **34** (8), 802–812.

Bagheri, S., Henningson, D. S., Hœpffner, J. & Schmid, PJ 2009 Input-output analysis and control design applied to a linear model of spatially developing flows. *Applied Mechanics Reviews* **62**, 020803.

Corke, T.C., Post, M.L. & Orlov, D.M. 2009 Single dielectric barrier discharge plasma enhanced aerodynamics: physics, modeling and applications. *Experiments in Fluids* **46** (1), 1–26.

Dadfar, R., Semeraro, O., Hanifi, A. & Henningson, D.S. 2013 Output feedback control of flow on a flat plate past a leadig edge using plasma actuators. *AIAA J.* Accepted for the publication.

Grundmann, S. & Tropea, C. 2008 Active cancellation of artificially introduced tollmien–schlichting waves using plasma actuators. *Experiments in Fluids* **44** (5), 795–806.

Joshi, S.S., Speyer, J.L. & Kim, J. 1997 A systems theory approach to the feedback stabilization of infinitesimal and finite-amplitude disturbances in plane poiseuille flow. *Journal of Fluid Mechanics* **332** (1), 157–184.

Juang, J.N. & Pappa, R.S. 1985 An eigensystem realization algorithm for modal parameter identification and model reduction. *Journal of Guidance* **8** (5), 620–627.

Kachanov, Yury S 1994 Physical mechanisms of laminar-boundary-layer transition. *Annual review of fluid mechanics* **26** (1), 411–482.

Kim, J. & Bewley, T.R. 2007 A linear systems approach to flow control. *Annu. Rev. Fluid Mech.* **39**, 383–417.

Kriegseis, J. 2011 Performance characterization and quantification of dielectric barrier discharge plasma actuators .

Maday, Y. & Patera, A.T. 1989 Spectral element methods for the incompressible navier-stokes equations. In *IN: State-of-the-art surveys on computational mechanics (A90-47176 21-64). New York, American Society of Mechanical Engineers, 1989, p. 71-143. Research supported by DARPA.*, , vol. 1, pp. 71–143.

Mertz, B.E. & Corke, T.C. 2011 Single-dielectric barrier discharge plasma actuator modelling and validation. *Journal of Fluid Mechanics* **669**, 557–583.

Moore, B. 1981 Principal component analysis in linear systems: Controllability, observability, and model reduction. *Automatic Control, IEEE Transactions on* **26** (1), 17–32.

Paul F. Fischer, James W. Lottes & Kerkemeier, Stefan G. 2008 nek5000 Web page. Http://nek5000.mcs.anl.gov.

Reed, A.D., Weismuller, M & Tropea, C. 2013 Free-flight investigation of transition under turbulent conditions on a laminar wing glove. AIAA 2013-0994.

Rowley, C.W. 2005 Model reduction for fluids, using balanced proper orthogonal decomposition. *International Journal of Bifurcation Chaos in Applied Sciences and Engineering* **15** (3), 997–1014.